Charge and valence bond orders in the spin-$\frac{1}{2}$ triangular antiferromagnet

Takashi Yamamoto,[1,2,3,*] Takashi Fujimoto,[1] Yasuhiro Nakazawa,[4] Masafumi Tamura,[5] Mikio Uruichi,[6] Yuka Ikemoto,[7]
Taro Moriwaki [7], HengBo Cui,[3,8] and Reizo Kato [3]

[1]*Graduate School of Science and Technology, Ehime University, 2-5 Bunkyocho, Matsuyama 7908577, Japan*
[2]*Geodynamics Research Center, Ehime University, Matsuyama 790-8577, Japan*
[3]*RIKEN, 2-1 Hirosawa, Wako 3510198, Japan*
[4]*Graduate School of Science, Osaka University, 1-1 Machikaneyama, Toyonaka 560-0043, Japan*
[5]*Department of Physics, Faculty of Science and Technology, Tokyo University of Science, 2641 Yamazaki, Noda 2788510, Japan*
[6]*Institute for Molecular Science, Okazaki 444-8585, Japan*
[7]*JASRI, SPring-8, 1-1-1 Kouto, Sayo, Hyogo 679-5198, Japan*
[8]*Institute of Applied Physics, Seoul National University, Seoul 08826, Korea*

Spin fluctuations play pivotal roles in condensed matter physics. Motivated by the discovery of valence bond order (VBO) -based fluctuations in superconductors and spin-liquid candidates, we investigated VBO within a molecule-based triangular lattice exhibiting antiferromagnetic order (AFO) in β'-EtMe$_3$As[Pd(dmit)$_2$]$_2$ using vibrational spectroscopy. The two triangular lattice layers of dimer ([Pd(dmit)$_2$]$_2^-$) units in the unit cell, separated by cationic EtMe$_3$As$^+$ layers, are crystallographically independent below the cation ordering temperature $T_{cat} = 230$ K. Below T_{cat}, part of the triangular lattice in both layers exhibits VBO fluctuations with inhomogeneous charges. At approximately 50 K, between T_{cat} and the antiferromagnetic transition temperature $T_{AF} = 23$ K, the VBO fluctuations in one layer freeze and coexist with frustrating 1/2 spins in the dimers. Conversely, the VBO fluctuations in the other layer cease simultaneously with the antiferromagnetic transition. In both layers, the frozen VBO (nonmagnetic tetramers) and spin-1/2 dimers coexist below T_{AF}. The results of this study reveal that hidden VBOs coexist in the AFO state.

I. INTRODUCTION

Antiferromagnetic (AF) fluctuations have attracted significant attention as potential drivers of unconventional superconductivity in two-dimensional (2D) inorganic and molecular conductors [1–5]. However, the concurrent presence of charge and lattice fluctuations observed in both *p*- and *n*-type cuprates [6–18], as well as in certain molecular superconductors [19–26], suggests the existence of a resonating valence bond. Similar fluctuations have been observed in spin-liquid (SL) candidates characterized by a triangular lattice, such as β'-EtMe$_3$Sb[Pd(dmit)$_2$]$_2$ (Et=Ethyl, Me=Methyl, dmit=1,3-dithiol-2-thione-4,5-dithiolate, and the symbol β' represents the arrangement type of [Pd(dmit)$_2$]$_2$ units) and κ-(ET)$_2$Cu$_2$CN$_3$ [ET=bis(ethylenedithio)tetrathiafulvalene] [27,28]. Therefore, to better understand quantum criticality, the antiferromagnetic order (AFO) and valence bond order (VBO) boundaries must be explored [15,29,30]. The AFO-VBO boundary has been investigated theoretically in honeycomb [31–34], square [35,36], and anisotropic triangular lattices [37–39]. In previous experimental investigations on molecule-based conductors, the VBO was substituted with AFO using external magnetic fields

[40–43]. However, the results obtained through magnetic field manipulation may differ from those obtained without a magnetic field [9,44]. In this study, we present compelling evidence that the VBO and AFO can be concurrently established within a molecule-based triangular lattice.

A series of anion radical salts derived from the Pd-dithiolene complex molecule, Et$_x$Me$_{4-x}$Z[Pd(dmit)$_2$]$_2$ [Z = N, P, As, and Sb], has garnered attention due to the observation of SL, AFO, VBO, and superconducting (SC) states achieved by tuning intermolecular interactions through pressure application or the selection of x and Z [45,46]. The molecular and crystal structures are shown in Fig. 1. The unit cell contained two anion layers (1 and 2) where the dimeric [Pd(dmit)$_2$]$_2$ units formed a triangular lattice. The dimer possessed one valence electron and a half-filled conduction band. The ground states of Et$_x$Me$_{4-x}$Z[Pd(dmit)$_2$]$_2$ can be classified based on the ratios of the interdimer transfer integrals corresponding to the three sides of the triangular lattice: t_S, t_T, and t_D [46,47]. Utilizing the simplified classification parameter $t_{AV} = (t_S + t_T)/2$, the AFO system satisfies $t_{AV} > 1.1 t_D$, the SL candidate emerges when $t_{AV} \approx 1.1 t_D$, and a nonmagnetic and charge-ordered (NMCO) state arises when $t_{AV} \approx t_D$ [46,47]. Investigations of *monoclinic*-EtMe$_3$P[Pd(dmit)$_2$]$_2$ and β'-Et$_2$Me$_2$Sb[Pd(dmit)$_2$]$_2$ have unveiled the nonuniformity of t_S and the intradimer transfer integral in the NMCO state due to the formation of VBO [48–50]. These findings indicate the need to reevaluate the SL and AFO states within
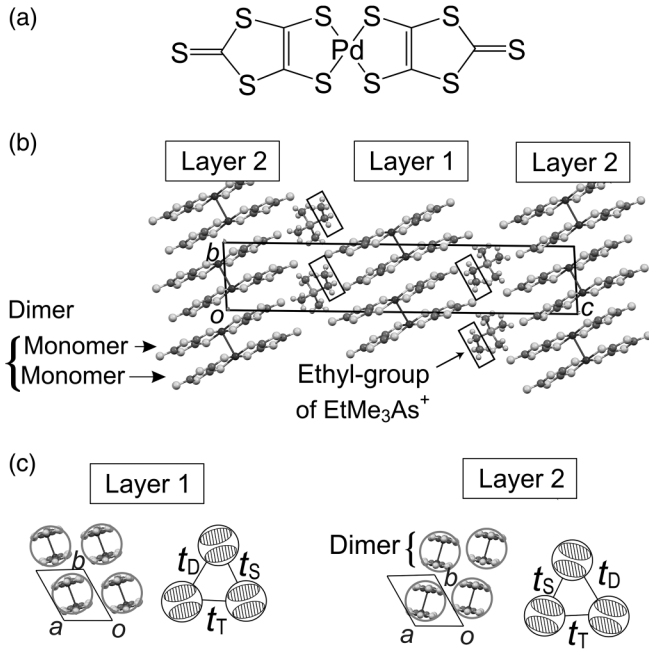
FIG. 1. (a) Structural formula of Pd(dmit)$_2$. (b) Crystal structure of β'-EtMe$_3$As[Pd(dmit)$_2$]$_2$ viewed along the **a**-axis at 5 K. Monomers Pd(dmit)$_2$ form dimer [Pd(dmit)$_2$]$_2$ in the conducting layers. The two conducting layers 1 and 2 are independent below the cation ordering transition temperature ($T_{cat} = 230$ K) because of the orientational disorder in the EtMe$_3$As$^+$ ions. (c) Projection and schematic of layers 1 and 2 viewed along the long axis of Pd(dmit)$_2$. Open circles and ellipses denote the dimer and monomer, respectively.

the context of VBO formation. In our prior investigation of the SL candidate β'-EtMe$_3$Sb[Pd(dmit)$_2$]$_2$, we demonstrated the emergence of dynamic fluctuations that originated from VBO accompanied by charge order [28]. Notably, the pnictogen atom Z in β'-EtMe$_3$As[Pd(dmit)$_2$]$_2$ was only one period smaller than that in the SL candidate, with the ground state of β'-EtMe$_3$As[Pd(dmit)$_2$]$_2$ identified as AFO [51]. We report compelling evidence of the coexistence of AFO and VBO within the same 2D layer of β'-EtMe$_3$As[Pd(dmit)$_2$]$_2$ as well as the simultaneous freezing of AFO and VBO. Henceforth, β'-EtMe$_3$As[Pd(dmit)$_2$]$_2$ is denoted as β'-As.

β'-As functions as a semiconductor under ambient pressure [51]. The magnetic susceptibility demonstrates an anisotropic response to external magnetic fields, indicating the onset of AFO at $T_{AF} = 23$ K [51]. An SC transition is observed at 4.3 K and 7 kbar [51]. In the 300 K structure (space group $C2/c$), layers 1 and 2 possess crystallographic equivalence, wherein the EtMe$_3$As$^+$ cation on the twofold axis shows orientational disorder. Layers 1 and 2 become independent in the triclinic lattice (space group $P\bar{1}$) below the cation ordering transition temperature ($T_{cat} = 230$ K), with the ethyl group of each cation facing layer 1 [51]. Based on x-ray structural data at 300 K, the extended Hückel calculations indicate that $t_S \approx t_T \approx 1.3\,t_D$, which possibly satisfies the condition of the pseudosquare lattice [46,47]. Although x-ray diffraction is useful for determining average and uniformly ordered structures, further analysis is required to detect random inhomogeneities

in the transfer integrals and site charges. Vibrational spectroscopy (VS) is an alternative. The C=C stretching modes of the dimer [Pd(dmit)$_2$]$_2$ exhibit peak splitting, regardless of whether the fluctuations in the transfer integrals and site charges are static or dynamic [20,52–56].

II. EXPERIMENT

The C=C stretching modes of β'-As were investigated using IR and Raman spectrometers. Polarized IR reflectance spectra were acquired using a spectrometer and an infrared microscope. At BL 43 IR in Spring-8, we employed Bruker Vertex 70 and Hyperion 2000, whereas we utilized a Nicolet Magna 760 FT-IR spectrometer and a Spectra-Tech IR-Plan microscope at the Institute of Molecular Science. The IR spectra were then transformed into conductivity spectra using the Kramers-Kronig transformation. In this paper, the conductivity spectrum is referred to as the IR spectrum. Raman spectra were recorded using a RENISHAW inVia Reflex system in a backscattering configuration. The laser polarization direction was parallel to the interplanar direction of the single crystal. The single crystals were cooled using a helium flow cryostat at a cooling rate of 1 K/min. The C=C stretching modes were measured at various temperatures ranging from 300 to 5 K. X-ray structural analysis of the single crystal was performed at 5 K since no x-ray data below T_{AF} have been published. The x-ray diffraction data were collected using a Weisenberg-type imaging plate system (R-AXIS RAPID/CS, Rigaku Corp.) with monochromated Mo $K\alpha$ radiation (UltraX6-E, Rigaku Corp.). The low-temperature experiments were performed in a closed-cycle helium refrigerator (HE05/UV404, ULVAC CRYOGENICS Inc.). The temperature was controlled by Model 22C Cryogenic Temperature Controller (Cryogenic Control Systems Inc.). All diffraction data were processed using the CrystalStructure 3.8 crystallographic software package. The structures were solved using the direct method (SIR92) and refined using the full-matrix least-squares method (SHELX- 2018/3) [57].

III. RESULTS

The results of the x-ray structure analysis performed at 5 K are summarized in the Supplemental Material [58]. In a previous study, the x-ray structure analysis was performed at 150 K [51], and no significant difference was observed between the 150 and 5 K structures. Although the x-ray diffraction method is useful for determining average, uniformly ordered structures, it is difficult to detect inhomogeneities in the transfer integrals and site charges using ordinary x-ray diffraction measurements. Therefore, the focus shifted to vibrational spectroscopy.

Figure 2 shows the IR and Raman spectra of β'-As at 300 K. The four C=C stretching modes in the dimer were denoted A_D^R, B_D^R, C_D^I, and D_D^R. Superscripts I and R indicate the IR- and Raman-active modes, respectively, whereas subscript D denotes a dimer-specific vibrational mode [53]. These spectra were consistent with the typical spectra of Et$_x$Me$_{4-x}$Z[Pd(dmit)$_2$]$_2$ at room temperature. To our knowledge, intradimer interaction is correlated with the behavior of D_D^R, whereas interdimer interaction and dimer charge are
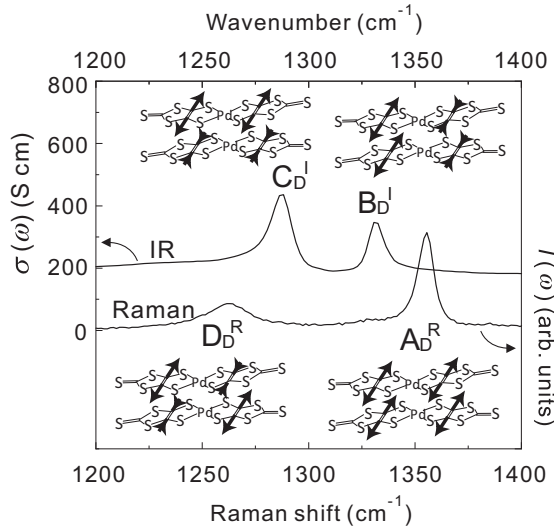
FIG. 2. IR and Raman spectra of β'-As at 300 K. Note that conductivity spectra are referred to as IR spectra in this article. The incident light of the IR spectra is polarized in the $(a + 2b)$-direction. The excitation light of the Raman spectra is a 514 nm laser. Four illustrations refer to vibrational motions of A_D^R, B_D^I, C_D^I, and D_D^R, in which the C=C bonds in dimer $[Pd(dmit)_2]_2$ are stretching and shrinking.

correlated with the behavior of A_D^R. Furthermore, the monomer charge was correlated with the frequency of B_D^I. It is expected that the inter- and intradimer interactions, along with the dimer and monomer charges at low temperatures, can be investigated from A_D^R, B_D^I, and D_D^R in the low-temperature spectra. However, our previous studies revealed that C_D^I does not provide useful information because its frequency and line shape are affected by all inter- and intradimer interactions, as well as dimer and monomer charges, making it nearly

impossible to separate these individual effects. Hereafter, we focus on the behaviors of A_D^R, B_D^I, and D_D^R.

Figure 3 shows the Raman spectra obtained at various temperatures using the (a) 514 nm, (b) 633 nm, and (c) 785 nm lasers. A_D^R and D_D^R showed peak separations at 200–220 K. The majority of C=C stretching modes observed at 5 K originated below T_{cat}. Curve fitting was applied to the 5 K spectra in the frequency regions containing A_{XD}^R, A_{XT}^R, D_{YD}^R, and D_{YT}^R. All attempts to fit on the assumption of a split into two peaks were unsuccessful. The results of the curve fitting applied to the 5 K spectra are superimposed in Fig. 4. The peak assignments were based on previous assignments for other $Et_xMe_{4-x}Z[Pd(dmit)_2]_2$ compounds, particularly assignments in the AFO state of β'-$Et_2Me_2P[Pd(dmit)_2]_2$ and the NMCO state of *triclinic* $EtMe_3P[Pd(dmit)_2]_2$, as shown in Fig. S1 in the Supplemental Material [28,50,58–61]. The subscripts X and Y denote the vibrational modes associated with layers X and Y, respectively, and subscript T denotes the tetramer modes. The unassigned peaks, which originated from C_D^I, are not shown in Fig. 4. Either layer X or Y corresponds to layer 1, whereas the others correspond to layer 2. Because the 633 nm laser does not resonate with neutral, monoanionic, or dianionic dimers [53], the relative intensity obtained using the 633 nm laser should be proportional to the number of dimers. As shown in the central spectrum in Fig. 4, the peak area represented by $A_{YD}^R + A_{YT}^R$ is equal to the sum of the areas of A_{XD}^R and A_{XT}^R. Similarly, the peak area represented by $D_{YD}^R + D_{YT}^R$ is equal to the sum of the areas of D_{XD}^R and D_{XT}^R. The same result was achieved using a 514 nm laser. We categorized the A_{XD}^R, A_{XT}^R, D_{XD}^R, and D_{XT}^R modes under layer X, whereas the A_{YD}^R, A_{YT}^R, D_{YD}^R, and D_{YT}^R modes were attributed to layer Y.

One might speculate that A_{XT}^R and A_{XD}^R are assigned to charge-rich and charge-poor dimers, similar to the NMCO state of β'-$Et_2Me_2Sb[Pd(dmit)_2]_2$ [62]. However, the frequency difference between A_{XT}^R and A_{XD}^R (5 cm^{-1}) was
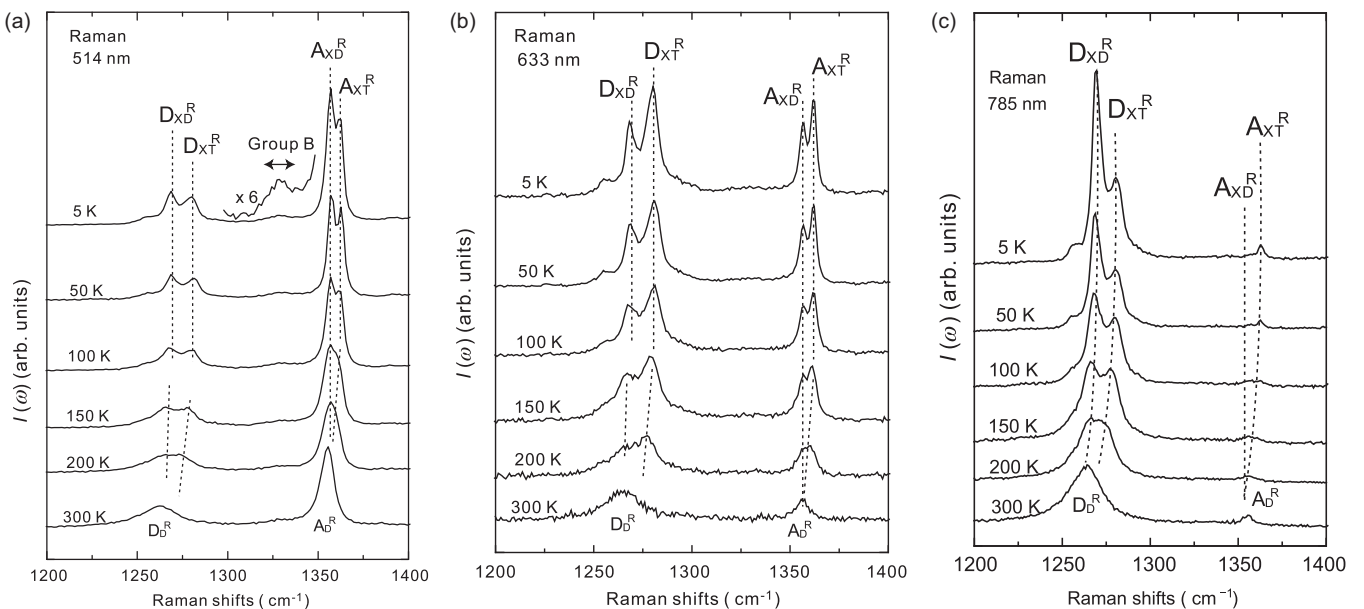

FIG. 3. Raman spectra at various temperatures of β'-As obtained using (a) 514 nm, (b) 633 nm, and (c) 785 nm lasers. Dashed lines are a guide for the eye.
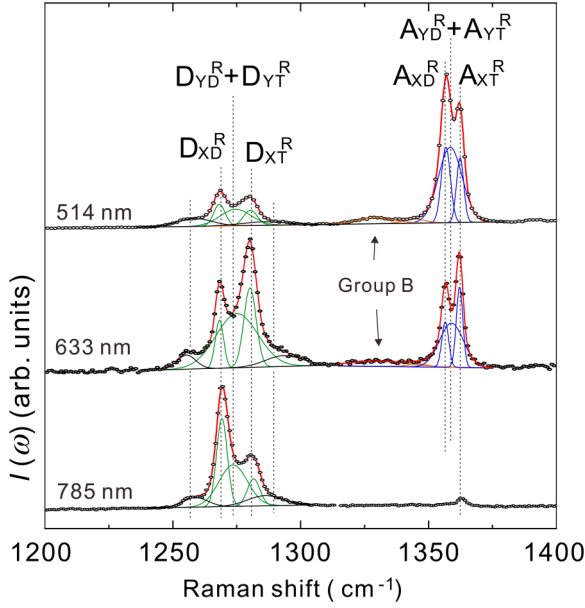
FIG. 4. Results of curve fittings applied to the Raman spectra at 5 K obtained using 514, 633, and 785 nm lasers. Dashed lines are a guide for the eye.

significantly smaller than that in the NMCO state of β'-Et$_2$Me$_2$Sb[Pd(dmit)$_2$]$_2$ (36 cm^{-1}) [59]. Furthermore, the frequency of A_{XD}^R was identical to that of the monovalent dimer [Pd(dmit)$_2$]$_2^-$, as well as to those in other β'-Et$_x$Me$_{4-x}$Z[Pd(dmit)$_2$]$_2$ compounds exhibiting the AFO state [28,53]. These results indicate that there is no charge-poor dimer in β'-As, and A_{XT}^R does not correspond to a charge-rich dimer. Studies on another type of NMCO state in *triclinic* EtMe$_3$P[Pd(dmit)$_2$]$_2$ have revealed that the frequency of the Raman mode corresponding to the A_{XT}^R mode is slightly higher (approximately 4 cm^{-1}) than that of [Pd(dmit)$_2$]$_2^-$ [60]. This phenomenon can be attributed to the appearance of charge-rich and charge-poor monomers in the dimer due to

tetramerization. The dimer charge in this type of NMCO state is -1. Table I presents the schematic views of the tetramers formed by dimer pairing. The similarity with the vibrational mode of *triclinic* EtMe$_3$P[Pd(dmit)$_2$]$_2$ indicates that two dimers in the tetramer vibrate in-phase in A_{XT}^R of β'-As. Conversely, the dimer vibrates independently in A_{XD}^R. This indicates that layer X comprises both tetramers and dimers. Observation of the D_{XT}^R and D_{XD}^R modes also indicates the coexistence of tetramers and dimers within layer X.

Next, we discuss the vibrational modes in layer Y. The linewidths of the peaks corresponding to $A_{YD}^R + A_{YT}^R$ and $D_{YD}^R + D_{YT}^R$ in Fig. 4 were 12 and 22 cm^{-1}, respectively. These values are four times larger than the A_D^R and D_D^R linewidths observed in other AF compounds; nonetheless, they can be compared to those of the corresponding modes in the SL candidate β'-EtMe$_3$Sb[Pd(dmit)$_2$]$_2$ [28]. For the SL candidate, this broad linewidth is attributed to the dynamic fluctuation between the dimers and two distinct types of NMCOs. In the case of β'-As, the frequency of $A_{YD}^R + A_{YT}^R$ is higher than the A_{XD}^R frequency but lower than the A_{XT}^R frequency, leading to the absence of a charge-rich or charge-poor dimer in layer Y. This indicates that $A_{YD}^R + A_{YT}^R$ encompasses both the A_{YD}^R and A_{YT}^R modes, as indicated in Table I, due to spatial and/or dynamic fluctuations between the tetramers and dimers. Similar to $A_{YD}^R + A_{YT}^R$, $D_{YD}^R + D_{YT}^R$ includes both D_{YD}^R and D_{YT}^R modes. The existence of inhomogeneous charges attributed to tetramerization should occur within dimers in layer Y, which will be examined elsewhere. No assignment was provided for the peaks at 1290 and 1255 cm^{-1} in Fig. 4 because those originate from the C_D^I mode.

The coexistence of tetramers and dimers in layer X was supported by other vibrational modes observed in the IR spectra. Figure 5 shows the conductivity spectra obtained from the 5 K and polarized IR spectra. Hereafter, the conductivity spectra are referred to as the IR spectra. The results of curve fitting applied to the $(a + 2b)$- and c^*-polarized spectra are superimposed in Fig. 5.

TABLE I. Assignments of the vibrational modes originating from the A_D^R, D_D^R, and B_D^I modes at 5 K. No assignment was provided for D_{XT}^I or D_{YT}^I due to their overlap with vibrational modes originating from C_D^I in Fig. 5. Open and filled ellipses in the tetramer illustrations denote the charge-poor and charge-rich molecules, respectively.

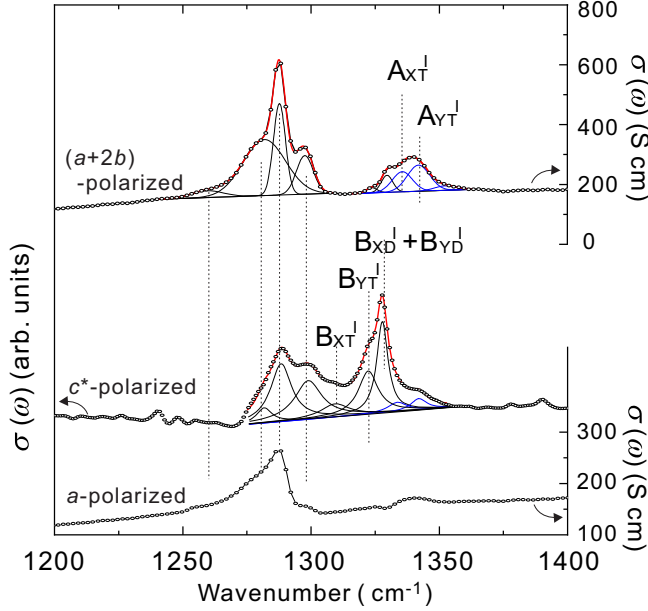|	Layer X				Layer Y			
	Dimer		Tetramer		Dimer		Tetramer	
Original mode of a dimer	Mode	ω (cm^{-1})	Mode	ω (cm^{-1})	Mode	ω (cm^{-1})	Mode	ω (cm^{-1})
A_D^R	A_{XD}^R	1357	A_{XT}^R	1362	A_{YD}^R	1359	A_{YT}^R	1359
			A_{XT}^I	1336			A_{YT}^I	1342
D_D^R	D_{XD}^R	1268	D_{XT}^R	1280	D_{YD}^R	1275	D_{YT}^R	1275
			D_{XT}^I				D_{YT}^I	
B_D^I	B_{XD}^I	1328	B_{XT}^R	Group B	B_{YD}^I	1328	B_{YT}^R	Group B
			B_{XT}^I	1310			B_{YT}^I	1322

FIG. 5. Conductivity spectra of β'-As at 5 K, those which are obtained from the $(a + 2b)$-, c^*-, and a-polarized IR reflectance spectra. Note that conductivity spectra are referred to as IR spectra in this article. Dashed lines are a guide for the eye.

The B_{XD}^I and B_{XT}^I modes originate from B_D^I, in which the frequency of B_D^I is proportional to the partial charge of the monomers in the dimer [53]. The frequency of the peak represented by $B_{XD}^I + B_{YD}^I$ in the c^*-polarized spectra was identical to that of $[Pd(dmit)_2]^{0.5-}$, indicating that layer X had independent dimers. In contrast, the frequency of B_{XT}^I corresponds to charge-poor monomers in the tetramer. By applying the tentative relationship between frequency (ω) and partial charge (ρ) $(d\omega/d\rho = -70/\text{electron})$ to the B_{XT}^I frequency [53,61], the partial charge of the charge-poor monomers in the tetramer was estimated as -0.24. Consequently, the partial charge of the charge-rich monomers in the tetramer was estimated as $-1 + 0.24 = -0.76$. Although the vibrational mode corresponding to the charge-rich monomer B_{XT}^R was observed in the region denoted as Group B in Figs. 3(a) and 4, its exact frequency could not be determined because of its weak intensity. In the preceding paragraph, A_{XT}^R was identified as the in-phase vibration of two dimers within a tetramer. Consequently, the out-of-phase vibration A_{XT}^I should manifest in the IR spectra, and its frequency should experience a redshift in comparison to A_{XT}^R due to the electron-molecular vibrational (e-mv) interaction. This corresponding mode, A_{XT}^I, was observed at $1336\,\text{cm}^{-1}$ in Fig. 2(c). These assignments provide conclusive evidence that layer X comprises both dimers and tetramers formed by charge-separated dimers.

The existence of inhomogeneous charges attributed to the tetramerization within layer Y was confirmed by the fact that the frequency of B_{YT}^I was lower than that of $[Pd(dmit)_2]^{0.5-}$. Based on the B_{YT}^I frequency, the partial charge of the charge-poor monomers in layer Y was estimated to be -0.41. Consequently, the partial charge of the charge-rich monomers is estimated to be $-1 + 0.41 = -0.59$. Although the corresponding B_{YT}^R mode was perceptible in the region identified

as Group-B in Figs. 3(a) and 4, its intensity was insufficient to determine its frequency precisely. The difference in partial charges in layer Y, $\Delta\rho = 0.18$, is smaller than that in layer X, $\Delta\rho = 0.32$. In addition, the mode represented by $B_{XD}^I + B_{YD}^I$ in the c^*-polarized spectra exhibits a notably higher intensity than the B_{YT}^I and B_{XT}^I modes. This observation strongly indicates that the mode $B_{XD}^I + B_{YD}^I$ encompasses both the B_{XD}^I and B_{YD}^I modes.

Assuming the presence of tetramers in layer Y, we expected to observe not only the A_{YT}^R but also the out-of-phase mode. Mode A_{YT}^I in Fig. 5 is identified as the out-of-phase mode. The degree of lattice distortion can be assessed by examining the frequency difference between the two e-mv modes, A_{YT}^R and A_{YT}^I. The frequency difference denoted as $\Delta A = \omega(A_{YT}^R) - \omega(A_{YT}^I) = 17\,\text{cm}^{-1}$ is smaller than the corresponding values in layer X, $\Delta A = \omega(A_{XT}^R) - \omega(A_{XT}^I) = 26\,\text{cm}^{-1}$. The values of ΔA and $\Delta\rho$ in layer Y are smaller than those in layer X. This observation aligns with our previous finding that ΔA is proportional to $\Delta\rho$ [53]. The intensity of A_{YT}^I at 5 K is nearly identical to that of A_{XT}^I; this suggests that the relative abundance of tetramers to dimers in layer Y at 5 K is comparable to that in layer X. No assignment was provided for the D_{XT}^I or D_{YT}^I mode in Table I due to their overlap with vibrational modes originating from the C_D^I mode in the frequency region between 1250 and $1300\,\text{cm}^{-1}$ in Fig. 5.

Figure 6 shows the IR spectra obtained at various temperatures. Figures 6(a) and 6(b) show an increase in the number of C=C stretching modes at temperatures below 200 K. The intensities of A_{XT}^I and A_{YT}^I in the 5 K spectra in Fig. 6(b) are smaller than those in Fig. 6(a), indicating that the tetramer is not formed in the transverse direction, as shown in Fig. 1. Tetramers should be formed along the stacking and/or diagonal directions, as discussed later. The asterisks in Fig. 6(c) indicate an increase in the number of vibrational modes originating from cations below 200 K. The emergence of A_{XT}^I in the 200 K spectra confirms that the tetramerization in layer X started below T_{cat}. The intensity of A_{YT}^I in the spectra at 24 K is weak. Furthermore, no trace of A_{YT}^I was observed in the 70 or 50 K spectrum; this suggests that the VBO in layer Y begins to freeze at the same temperature as T_{AF}. However, the charge-sensitive vibrational mode of B_{YT}^I persists even at 200 K. A similar precursor behavior originating from the B_D^I mode was observed in the SL candidate β'-EtMe$_3$Sb[Pd(dmit)$_2$]$_2$ [28]. The difference in the partial charges in layer Y, $\Delta\rho = 0.18$, is also comparable to that in the SL candidate, $\Delta\rho = 0.14$ [28]. These results indicate that the dynamic fluctuation between the tetramers and dimers in layer Y occurs in the temperature range between T_{cat} and T_{AF}. Both tetramers and dimers in layer Y begin to freeze at T_{AF}.

IV. DISCUSSION

The results demonstrate the coexistence of tetramers, characterized by the formation of the VBO state, and dimers in both layers X and Y at 5 K. The presence of the VBO suggests anisotropic contraction of the triangular lattice. Using x-ray structural analysis at 5 K, we estimated the parameters t_S, t_T, and t_D. As shown in Table II, t_S is larger than t_T and t_D in both layers 1 and 2 at 5 K, thereby confirming the anisotropy of both layers and that the electron-phonon
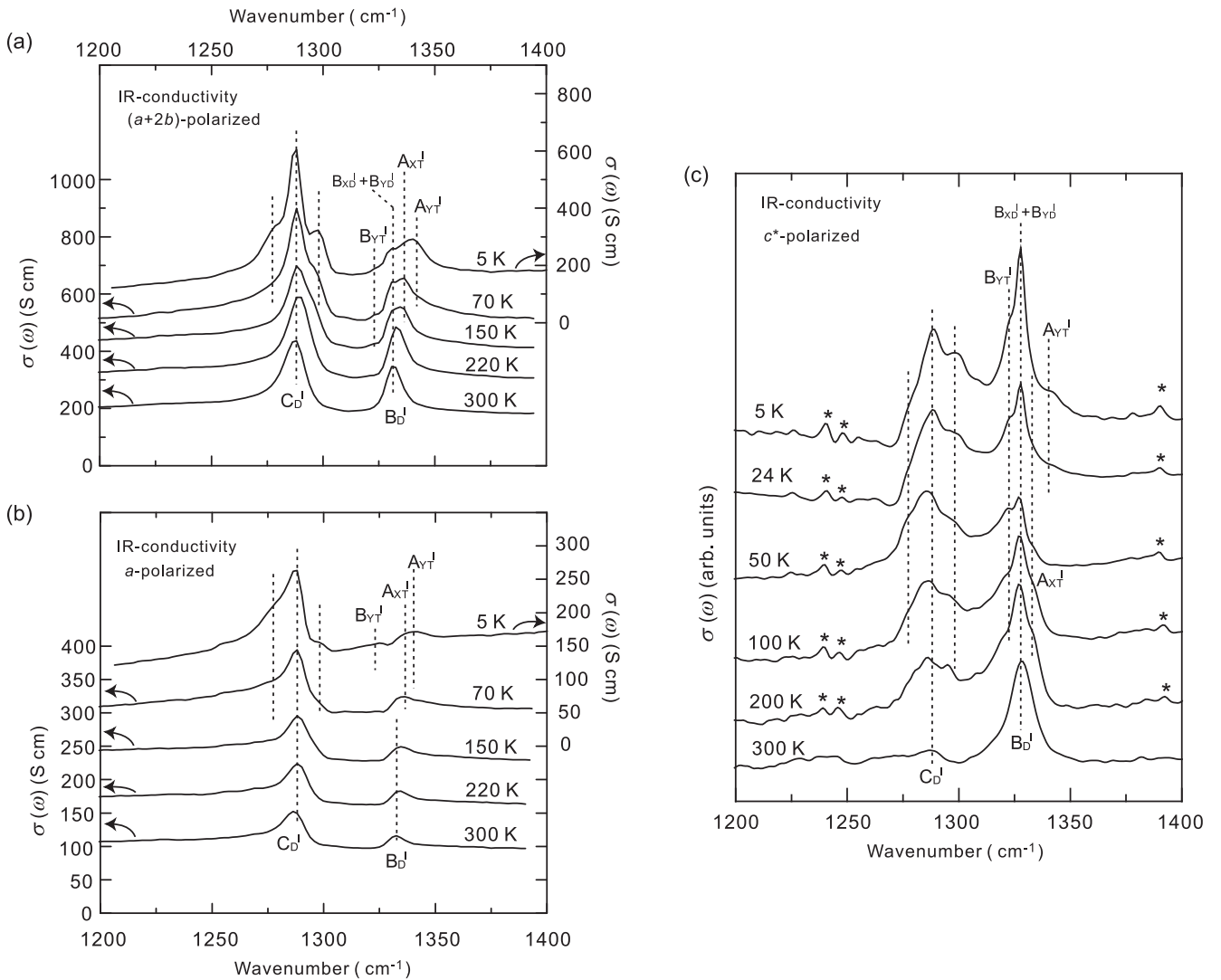
FIG. 6. Conductivity spectra obtained from the (a) $(a + 2b)$-, (b) a-, and (c) c^*-polarized IR-reflectance spectra. The spectra at 220, 150, and 70 K in (a) are offset by 100 S cm^{-1}. The spectra at 220, 150, and 70 K in (b) are offset by 50 S cm^{-1}. Asterisks in (c) indicate the vibrational modes that originate from cation ordering.

interaction operates along the stacking direction; this is similar to observations in previous studies on *triclinic* and *monoclinic* EtMe$_3$P[Pd(dmit)$_2$]$_2$, where the instability arising from the HOMO-LUMO inversion in the tight dimer was resolved through the formation of a VBO along the stacking direction [50,60]. We also briefly discuss cation ordering. In the NMCO state of *triclinic* EtMe$_3$P[Pd(dmit)$_2$]$_2$, the ethyl groups also face one of the two independent layers [60]. This similarity implies that the steric effect of the ethyl groups and the electron-phonon interactions synergistically contribute to the formation of an anisotropic triangular lattice.

TABLE II. Interdimer transfer integrals t_S, t_T, and t_D in β'-As calculated using the results of the x-ray analyses at 5 and 300 K.

Layer	t_S (meV)	t_T (meV)	t_D (meV)
Layer 1 at 5 K	43.3	37.8	25.9
Layer 2 at 5K	45.3	39.4	29.6
Layers 1 and 2 at 300 K [51]	30.5	30.3	23.2

One of the candidates for the 2D structure of each layer at 5 K is the periodic alignment of tetramers and dimers, resembling a threefold structure induced by electron-electron repulsion [63]. However, in practice, electron-phonon interactions should also be considered [64,65]. Furthermore, in the AFO states of other β'-Et$_x$Me$_{4-x}$Z[Pd(dmit)$_2$]$_2$ compounds, the intensity of the peak corresponding to A_{XD}^R is approximately one order of magnitude larger than that of the peak corresponding to A_{XT}^R [28], which contradicts the hypothesis of the threefold periodic alignment. Another possible mechanism involves the formation of domains consisting of dimers and tetramers. However, IR and Raman mapping with a spatial resolution of $10 \times 10\,\mu\text{m}^2$ did not reveal any significant difference in peak intensities between dimers and tetramers; this suggests the presence of nanoscale domains or a solid-solution-like state in which the dimers and tetramers are randomly arranged in the same 2D layer. Further experimental and theoretical investigations are required to elucidate the detailed structure of the 2D arrangements.

We compared the results obtained from the vibrational spectroscopy with the temperature dependence of the magnetic susceptibility $\chi(T)$, as presented in the Supplemental Material of a previous article [51]. The $\chi(T)$ data revealed a small decrease at T_{cat}, which aligned with the observation that the VBO state in layer X begins to form at T_{cat}. However, $\chi(T)$ did not exhibit a steep decrease in the spin-Peierls transition but roughly followed the behavior expected from the Heisenberg triangular AF model between 300 and 50 K, similar to the $\chi(T)$ data of the SL candidate β'-EtMe$_3$Sb[Pd(dmit)$_2$]$_2$ [66,67]. The results of curve fitting applied to the 514 and 633 nm spectra in Fig. 4 demonstrated that at least half of all dimers in layer X possessed localized spins, whereas layer Y exhibited similar frustration as the SL candidate β'-EtMe$_3$Sb[Pd(dmit)$_2$]$_2$. Consequently, at least 3/4 of all dimers had $S = 1/2$ spins between T_{cat} and T_{AF}, which was consistent with the $\chi(T)$ behavior between 300 and 50 K. Anisotropic behavior was observed for $\chi(T)$ below T_{AF}, and the A$_{YT}^I$ mode began to emerge below T_{AF}. Because the tetramers in layer Y were frozen below T_{AF}, the dimers were also fixed, indicating that the localized spins of the dimers in layers Y and X can form 3D magnetic ordering below the temperature of VBO formation in layer Y. β'-As is the molecule-based triangular lattice system that exhibits both VBO and AFO without an external field. Similarly, the IR and Raman spectra in the AFO states of some β'-Et$_x$Me$_{4-x}$Z[Pd(dmit)$_2$]$_2$ compounds showed vibrational modes that cannot be assigned to those of the dimers [28]. This indicates the coexistence of AFO and VBO states. Additional data must be accumulated to conclude whether these sequential and partial changes are a transition, crossover, or phase separation. An inhomogeneous electrical structure was also implied in κ-(ET)$_2$Cu[N(CN)$_2$]Br after rapid cooling, as well as by the thermal conductivity of κ-(ET)$_2$Hg(SCN)$_2$Br [68–70]. Related compounds with a triangular lattice, κ-(ET)$_2$Cu$_2$(CN)$_3$ and κ-(ET)$_2$B(CN)$_4$, exhibit the VBO state, and charge ordering was observed in κ-(ET)$_2$Hg(SCN)$_2$Cl [27,71–73]. These reports suggest that the possible presence of the VBO state should be investigated in the AFO state of all molecular-based triangular-lattice systems using experimental methods without the application of a magnetic field. In the present experiment, clear evidence for the coexistence was obtained through molecular vibration measurements, a particularly effective method for detecting mixed ground states. This experiment also demonstrates that the phenomenon is general, not limited to κ-BEDT-TTF salts.

In conclusion, β'-As exhibits the coexistence of dimers and charge-separated tetramers within the same layer. The freezing of the VBO in one of the two independent layers occurs below the temperature of cation ordering, T_{cat}, whereas in the other layer, freezing of the VBO and AFO occurs simultaneously at T_{AF}.

ACKNOWLEDGMENTS

[1] A. Chubukov, D. Pines, and J. Schmalian, *A Spin Fluctuation Model for d-wave Superconductivity, The Physics of Superconductors* (Springer, Berlin, 2003), pp. 495–590.

[2] E. Dagotto, Correlated electrons in high-temperature superconductors, Rev. Mod. Phys. **66**, 763 (1994).

[3] E. Demler, W. Hanke, and S.-C. Zhang, SO (5) theory of antiferromagnetism and superconductivity, Rev. Mod. Phys. **76**, 909 (2004).

[4] B. Kyung and A.-M. Tremblay, Mott transition, antiferromagnetism, and d-wave superconductivity in two-dimensional organic conductors, Phys. Rev. Lett. **97**, 046402 (2006).

[5] D. J. Scalapino, A common thread: The pairing interaction for unconventional superconductors, Rev. Mod. Phys. **84**, 1383 (2012).

[6] P. Abbamonte, A. Rusydi, S. Smadici, G. Gu, G. Sawatzky, and D. Feng, Spatially modulated 'mottness' in La$_{2-x}$Ba$_x$CuO$_4$, Nat. Phys. **1**, 155 (2005).

[7] P. W. Anderson, The resonating valence bond state in La$_2$CuO$_4$ and superconductivity, Science **235**, 1196 (1987).

[8] R. Arpaia, S. Caprara, R. Fumagalli, G. De Vecchi, Y. Peng, E. Andersson, D. Betto, G. De Luca, N. Brookes, and F. Lombardi, Dynamical charge density fluctuations pervading the phase diagram of a Cu-based high-T$_c$ superconductor, Science **365**, 906 (2019).

[9] E. Blackburn, J. Chang, M. Hücker, A. T. Holmes, N. B. Christensen, R. Liang, D. A. Bonn, W. N. Hardy, U. Rütt, and O. Gutowski, X-ray diffraction observations of a charge-density-wave order in superconducting ortho-II YBa$_2$Cu$_3$O$_{6.54}$ single crystals in zero magnetic field, Phys. Rev. Lett. **110**, 137004 (2013).

[10] J. Chang, E. Blackburn, A. Holmes, N. Christensen, J. Larsen, J. Mesot, R. Liang, D. Bonn, W. Hardy, and A. Watenphul, Direct observation of competition between superconductivity and charge density wave order in YBa$_2$Cu$_3$O$_{6.67}$, Nat. Phys. **8**, 871 (2012).

[11] R. Comin, R. Sutarto, E. da Silva Neto, L. Chauviere, R. Liang, W. Hardy, D. Bonn, F. He, G. Sawatzky, and A. Damascelli, Broken translational and rotational symmetry via charge stripe order in underdoped YBa$_2$Cu$_3$O$_{6+y}$, Science **347**, 1335 (2015).

[12] E. H. da Silva Neto, R. Comin, F. He, R. Sutarto, Y. Jiang, R. L. Greene, G. A. Sawatzky, and A. Damascelli, Charge ordering in the electron-doped superconductor Nd$_{2-x}$Ce$_x$CuO$_4$, Science **347**, 282 (2015).

[13] G. Ghiringhelli, M. Le Tacon, M. Minola, S. Blanco-Canosa, C. Mazzoli, N. Brookes, G. De Luca, A. Frano, D. Hawthorn,

and F. He, Long-range incommensurate charge fluctuations in (Y, Nd) $Ba_2Cu_3O_{6+x}$, Science **337**, 821 (2012).

[14] S. Johnston, I. M. Vishik, W. S. Lee, F. Schmitt, S. Uchida, K. Fujita, S. Ishida, N. Nagaosa, Z. X. Shen, and T. P. Devereaux, Evidence for the importance of extended Coulomb interactions and forward scattering in cuprate superconductors, Phys. Rev. Lett. **108**, 166404 (2012).

[15] M. Kang, J. Pelliciari, A. Frano, N. Breznay, E. Schierle, E. Weschke, R. Sutarto, F. He, P. Shafer, and E. Arenholz, Evolution of charge order topology across a magnetic phase transition in cuprate superconductors, Nat. Phys. **15**, 335 (2019).

[16] S. A. Kivelson, I. P. Bindloss, E. Fradkin, V. Oganesyan, J. Tranquada, A. Kapitulnik, and C. Howald, How to detect fluctuating stripes in the high-temperature superconductors, Rev. Mod. Phys. **75**, 1201 (2003).

[17] Y. Kohsaka, C. Taylor, K. Fujita, A. Schmidt, C. Lupien, T. Hanaguri, M. Azuma, M. Takano, H. Eisaki, and H. Takagi, An intrinsic bond-centered electronic glass with unidirectional domains in underdoped cuprates, Science **315**, 1380 (2007).

[18] J. M. Tranquada, B. J. Sternlieb, J. D. Axe, Y. Nakamura, and S. Uchida, Evidence for stripe correlations of spins and holes in copper oxide superconductors, Nature (London) **375**, 561 (1995).

[19] A. F. Bangura, A. I. Coldea, J. Singleton, A. Ardavan, A. Akutsu-Sato, H. Akutsu, S. S. Turner, P. Day, T. Yamamoto, and K. Yakushi, Robust superconducting state in the low-quasiparticle-density organic metals β''-(BEDT-TTF)$_4$[(H$_3$O)M(C$_2$O$_4$)$_3$] · Y: Superconductivity due to proximity to a charge-ordered state, Phys. Rev. B **72**, 014543 (2005).

[20] A. Girlando, M. Masino, J. A. Schlueter, N. Drichko, S. Kaiser, and M. Dressel, Charge-order fluctuations and superconductivity in two-dimensional organic metals, Phys. Rev. B **89**, 174503 (2014).

[21] Y. Ihara, M. Jeong, H. Mayaffre, C. Berthier, M. Horvatić, H. Seki, and A. Kawamoto, C 13 NMR study of the charge-ordered state near the superconducting transition in the organic superconductor β''-(BEDT-TTF)$_4$[(H$_3$O)Ga(C$_2$O$_4$)$_3$] · C$_6$H$_5$NO$_2$, Phys. Rev. B **90**, 121106(R) (2014).

[22] S. Mazumdar and R. Clay, Quantum critical transition from charge-ordered to superconducting state in the negative-U extended Hubbard model on a triangular lattice, Phys. Rev. B **77**, 180515(R) (2008).

[23] S. Mazumdar, R. T. Clay, and D. K. Campbell, Bond-order and charge-density waves in the isotropic interacting two-dimensional quarter-filled band and the insulating state proximate to organic superconductivity, Phys. Rev. B **62**, 13400 (2000).

[24] S. Mazumdar and R. T. Clay, The chemical physics of unconventional superconductivity, Int. J. Quantum Chem. **114**, 1053 (2014).

[25] T. Yamamoto, H. M. Yamamoto, R. Kato, M. Uruichi, K. Yakushi, H. Akutsu, A. Sato-Akutsu, A. Kawamoto, S. S. Turner, and P. Day, Inhomogeneous site charges at the boundary between the insulating, superconducting, and metallic phases of β''-type bis-ethylenedithio-tetrathiafulvalene molecular charge-transfer salts, Phys. Rev. B **77**, 205120 (2008).

[26] Y. Shimizu, H. Akimoto, H. Tsujii, A. Tajima, and R. Kato, Mott transition in a valence-bond solid insulator with a triangular lattice, Phys. Rev. Lett. **99**, 256403 (2007).

[27] B. Miksch, A. Pustogow, M. J. Rahim, A. A. Bardin, K. Kanoda, J. A. Schlueter, R. Hübner, M. Scheffler, and M. Dressel, Gapped magnetic ground state in quantum spin liquid candidate κ-(BEDT-TTF)$_2$Cu$_2$(CN)$_3$, Science **372**, 276 (2021).

[28] T. Yamamoto, T. Fujimoto, T. Naito, Y. Nakazawa, M. Tamura, K. Yakushi, Y. Ikemoto, T. Moriwaki, and R. Kato, Charge and lattice fluctuations in molecule-based spin liquids, Sci. Rep. **7**, 12930 (2017).

[29] E. H. da Silva Neto, M. Minola, B. Yu, W. Tabis, M. Bluschke, D. Unruh, H. Suzuki, Y. Li, G. Yu, and D. Betto, Coupling between dynamic magnetic and charge-order correlations in the cuprate superconductor Nd$_{2-x}$Ce$_x$CuO$_4$, Phys. Rev. B **98**, 161114(R) (2018).

[30] T. Ohgoe and M. Imada, Competition among superconducting, antiferromagnetic, and charge orders with intervention by phase separation in the 2D Holstein-Hubbard model, Phys. Rev. Lett. **119**, 197001 (2017).

[31] K. Harada, T. Suzuki, T. Okubo, H. Matsuo, J. Lou, H. Watanabe, S. Todo, and N. Kawashima, Possibility of deconfined criticality in SU (N) Heisenberg models at small N, Phys. Rev. B **88**, 220408(R) (2013).

[32] S. Pujari, K. Damle, and F. Alet, Néel-state to valence-bond-solid transition on the honeycomb lattice: Evidence for deconfined criticality, Phys. Rev. Lett. **111**, 087203 (2013).

[33] M. Weber, Valence bond order in a honeycomb antiferromagnet coupled to quantum phonons, Phys. Rev. B **103**, L041105 (2021).

[34] A. Albuquerque, D. Schwandt, B. Hetenyi, S. Capponi, M. Mambrini, and A. Läuchli, Phase diagram of a frustrated quantum antiferromagnet on the honeycomb lattice: Magnetic order versus valence-bond crystal formation, Phys. Rev. B **84**, 024406 (2011).

[35] R. G. Melko and R. K. Kaul, Scaling in the fan of an unconventional quantum critical point, Phys. Rev. Lett. **100**, 017203 (2008).

[36] A. W. Sandvik, Continuous quantum phase transition between an antiferromagnet and a valence-bond solid in two dimensions: Evidence for logarithmic corrections to scaling, Phys. Rev. Lett. **104**, 177201 (2010).

[37] M. Laubach, R. Thomale, C. Platt, W. Hanke, and G. Li, Phase diagram of the Hubbard model on the anisotropic triangular lattice, Phys. Rev. B **91**, 245125 (2015).

[38] A. Szasz and J. Motruk, Phase diagram of the anisotropic triangular lattice Hubbard model, Phys. Rev. B **103**, 235132 (2021).

[39] S. Dayal, R. T. Clay, H. Li, and S. Mazumdar, Paired electron crystal: Order from frustration in the quarter-filled band, Phys. Rev. B **83**, 245106 (2011).

[40] D. S. Chow, P. Wzietek, D. Fogliatti, B. Alavi, D. J. Tantillo, C. A. Merlic, and S. E. Brown, Singular behavior in the pressure-tuned competition between spin-Peierls and antiferromagnetic ground states of (TMTTF)$_2$PF$_6$, Phys. Rev. Lett. **81**, 3984 (1998).

[41] N. Matsunaga, S. Hirose, N. Shimohara, T. Satoh, T. Isome, M. Yamomoto, Y. Liu, A. Kawamoto, and K. Nomura, Charge ordering and antiferromagnetism in (TMTTF)$_2$SbF$_6$, Phys. Rev. B **87**, 144415 (2013).

[42] Y. Shimizu, M. Maesato, M. Yoshida, M. Takigawa, M. Itoh, A. Otsuka, H. Yamochi, Y. Yoshida, G. Kawaguchi, and D. Graf, Magnetic field driven transition between valence bond solid and antiferromagnetic order in a distorted triangular lattice, Phys. Rev. Res. **3**, 023145 (2021).

[43] W. Yu, F. Zhang, F. Zamborszky, B. Alavi, A. Baur, C. Merlic, and S. Brown, Electron-lattice coupling and broken symmetries of the molecular salt (TMTTF)$_2$SbF$_6$, Phys. Rev. B **70**, 121101(R) (2004).

[44] T. Yamamoto, T. Naito, M. Uruichi, H. Akutsu, and Y. Nakazawa, Lattice and charge fluctuations in a molecular superconductor, J. Phys. Soc. Jpn. **90**, 063708 (2021).

[45] R. Kato, Conducting metal dithiolene complexes: Structural and electronic properties, Chem. Rev. **104**, 5319 (2004).

[46] R. Kato, Development of π-electron systems based on [M(dmit)$_2$] (M=Ni and Pd; dmit: 1,3-dithiole-2-thione-4, 5-dithiolate) anion radicals, Bull. Chem. Soc. Jpn. **87**, 355 (2014).

[47] R. Kato and C. Hengbo, Cation dependence of crystal structure and band parameters in a series of molecular conductors, β'-(Cation)[Pd(dmit)$_2$]$_2$ (dmit=1,3-dithiole-2-thione-4,5-dithiolate), Cryst. **2**, 861 (2012).

[48] Y. Ishii, M. Tamura, and R. Kato, Magnetic study of pressure-induced superconductivity in the [Pd(dmit$_2$)] salt with spin-gapped ground state, J. Phys. Soc. Jpn. **76**, 033704 (2007).

[49] M. Tamura, A. Tajima, and R. Kato, Novel phase transition in Et$_2$Me$_2$Sb[Pd(dmit)$_2$]$_2$ at 70 K: A possible mechanism based on strong dimerization of two-level molecules, Synth. Met. **152**, 397 (2005).

[50] T. Yamamoto, Y. Nakazawa, M. Tamura, A. Nakao, A. Fukaya, R. Kato, and K. Yakushi, Property of the valence-bond ordering in molecular superconductor with a quasi-triangular lattice, J. Phys. Soc. Jpn. **83**, 053703 (2014).

[51] R. Kato, A. Tajima, A. Nakao, and M. Tamura, Two pressure-induced superconducting anion radical salts exhibiting different spin states at ambient pressure, J. Am. Chem. Soc. **128**, 10016 (2006).

[52] T. Yamamoto, Vibrational spectra of β''-type BEDT-TTF salts: Relationship between conducting property, time-averaged site charge and inter-molecular distance, Cryst. **2**, 893 (2012).

[53] T. Yamamoto, Diversity in electronic phase due to interchange of MO levels in [M(dmit)$_2$] anion salts (M = Pd and Pt), in *Functional Materials: Advances and Applications in Energy Storage and Conversion*, edited by T. Naito (Pan Stanford, Singapore, 2018), pp. 83–155.

[54] N. M. Hassan, K. Thirunavukkuarasu, Z. Lu, D. Smirnov, E. I. Zhilyaeva, S. Torunova, R. N. Lyubovskaya, and N. Drichko, Melting of charge order in the low-temperature state of an electronic ferroelectric-like system, npj Quantum Mater. **5**, 15 (2020).

[55] A. Pustogow, Y. Saito, A. Rohwer, J. Schlueter, and M. Dressel, Coexistence of charge order and superconductivity in β''-(BEDT-TTF)$_2$SF$_5$CH$_2$CF$_2$SO$_3$, Phys. Rev. B **99**, 140509(R) (2019).

[56] A. Girlando, M. Masino, S. Kaiser, Y. Sun, N. Drichko, M. Dressel, and H. Mori, Spectroscopic characterization of charge order fluctuations in BEDT-TTF metals and superconductors, Phys. Status Solidi B **249**, 953 (2012).

[57] G. M. Sheldrick, A short history of SHELX, Acta Cryst. A **64**, 112 (2008).

[58] Supplemental Material at http://link.aps.org/supplemental/10.1103/PhysRevB.110.205126 for he x-ray crystallographic data of β'-EtMe$_3$As[Pd(dmit)$_2$]$_2$ at 5 K and the C=C stretching modes of β'-Et$_2$Me$_2$P[Pd(dmit)$_2$]$_2$ and triclinic EtMe$_3$P[Pd(dmit)$_2$]$_2$.

[59] T. Yamamoto, Y. Nakazawa, M. Tamura, T. Fukunaga, R. Kato, and K. Yakushi, Vibrational spectra of [Pd(dmit)2] dimer (dmit = 1,3-dithiole-2-thione-4,5-dithiolate): Methodology for examining charge, inter-molecular interactions, and orbital, J. Phys. Soc. Jpn. **80**, 074717 (2011).

[60] T. Yamamoto, Y. Nakazawa, M. Tamura, A. Nakao, Y. Ikemoto, T. Moriwaki, A. Fukaya, R. Kato, and K. Yakushi, Intradimer charge disproportionation in triclinic-EtMe$_3$P[Pd(dmit)$_2$]$_2$ (dmit: 1,3-dithiole-2-thione-4,5-dithiolate), J. Phys. Soc. Jpn. **80**, 123709 (2011).

[61] T. Yamamoto, M. Tamura, K. Yakushi, and R. Kato, Intra- versus inter-dimer charge inhomogeneity in the triangular lattice compounds of β'-Cs[Pd(dmit)$_2$]$_2$ and β'-Et2Me$_2$Sb[Pd(dmit)$_2$]$_2$: A degree of freedom specific to an interchange of energy levels in the molecular orbitals, J. Phys. Soc. Jpn. **85**, 104711 (2016).

[62] A. Nakao and R. Kato, Structural study of low temperature charge-separated phases of Pd(dmit)$_2$-based molecular conductors, J. Phys. Soc. Jpn. **74**, 2754 (2005).

[63] H. Watanabe, H. Seo, and S. Yunoki, Phase competition and superconductivity in κ-(BEDT-TTF)$_2$X: Importance of inter-molecular coulomb interactions, J. Phys. Soc. Jpn. **86**, 033703 (2017).

[64] R. T. Clay, N. Gomes, and S. Mazumdar, Theory of triangular lattice quasi-one-dimensional charge-transfer solids, Phys. Rev. B **100**, 115158 (2019).

[65] W. W. De Silva, N. Gomes, S. Mazumdar, and R. T. Clay, Coulomb enhancement of superconducting pair-pair correlations in a 3/4-filled model for κ-(BEDT-TTF)$_2$X, Phys. Rev. B **93**, 205111 (2016).

[66] T. Itou, A. Oyamada, S. Maegawa, M. Tamura, and R. Kato, Quantum spin liquid in the spin-1/2 triangular antiferromagnet EtMe$_3$Sb[Pd(dmit)$_2$]$_2$, Phys. Rev. B **77**, 104413 (2008).

[67] M. Tamura and R. Kato, Magnetic susceptibility of β'-[Pd(dmit)$_2$] salts (dmit=1,3-dithiol-thione-4,5-dithiolate, C$_3$S$_5$): Evidence for frustration in spin-1/2 Heisenberg antiferromagnets on a triangular lattice, J. Phys.: Condens. Matter. **14**, L729 (2002).

[68] T. Sasaki, N. Yoneyama, N. Kobayashi, Y. Ikemoto, and H. Kimura, Imaging Phase Separation near the Mott Boundary of the Correlated Organic Superconductors κ-(BEDT-TTF)$_2$X, Phys. Rev. Lett. **92**, 227001 (2004).

[69] N. Yoneyama, T. Sasaki, N. Kobayashi, Y. Ikemoto, and H. Kimura, Phase separation in the vicinity of the surface of κ-(BEDT-TTF)$_2$Cu[N(CN)$_2$]Br by fast cooling, Phys. Rev. B **72**, 214519 (2005).

[70] M. Yamashita, S. Sugiura, A. Ueda, S. Dekura, T. Terashima, S. Uji, Y. Sunairi, H. Mori, E. I. Zhilyaeva, and S. A. Torunova, Ferromagnetism out of charge fluctuation of strongly correlated electrons in κ-(BEDT-TTF)$_2$Hg(SCN)$_2$Br, npj Quantum Mater. **6**, 87 (2021).

[71] Y. Yoshida, H. Ito, M. Maesato, Y. Shimizu, H. Hayama, T. Hiramatsu, Y. Nakamura, H. Kishida, T. Koretsune, and C. Hotta, Spin-disordered quantum phases in a quasi-one-dimensional triangular lattice, Nat. Phys. **11**, 679 (2015).

[72] N. Drichko, R. Beyer, E. Rose, M. Dressel, J. A. Schlueter, S. A. Turunova, E. I. Zhilyaeva, and R. N. Lyubovskaya, Metallic state and charge-order metal-insulator transition in the quasi-two-dimensional conductor κ-(BEDT-TTF)$_2$Hg(SCN)$_2$Cl, Phys. Rev. B **89**, 075133 (2014).

[73] N. Drichko, S. Sugiura, M. Yamashita, A. Ueda, S. Uji, N. Hassan, Y. Sunairi, H. Mori, E. I. Zhilyaeva, and S. Torunova, Charge and spin interplay in a molecular-dimer-based organic Mott insulator, Phys. Rev. B **106**, 064202 (2022).